Asymmetric Electron Energy Loss in Drift-Current Biased Graphene

Filipa R. Prudêncio [1,2] · Mário G. Silveirinha [1]

Abstract

The electric drift-current bias was recently introduced as a new paradigm to break the Lorentz reciprocity in graphene. Here, we study the impact of the nonreciprocal response in the energy extracted from a beam of swift charges traveling in the vicinity of a graphene sheet with drifting electrons. It is demonstrated that the drift bias leads to an asymmetric electron-energy-loss spectrum that depends on the sign of the charge velocity. It is found that when the drift and electron beam velocities have comparable values but opposite signs, the energy loss is boosted resulting in a noncontact friction-type effect. In contrast, when the drift and electron beam velocities have the same sign, the energy loss is negligible. Furthermore, it is shown that different theoretical models of the drift-biased graphene conductivity yield distinct peaks for the energy-loss spectrum, and thereby electron beam spectroscopy can be used to test the validity of the different theories.

Keywords Graphene plasmons · Nanophotonics · Electron energy-loss spectroscopy (EELS) · Drift-current bias · Nonreciprocity

Introduction

Nonreciprocal photonic platforms have been extensively investigated in the literature and offer unique opportunities to control electromagnetic wave propagation [1–9]. In particular, gyrotropic material structures can enable one-way light flows due to the nonreciprocal response of the involved materials [1–8]. Such solutions require an external magnetic bias to break the Lorentz reciprocity, which is often impractical [10, 11]. Systems relying on nonlinear effects [12, 13], opto-mechanical interactions [14–16], transistor-loaded metamaterials [17, 18], or spacetime modulations [19–22] offer alternative solutions to produce strong nonreciprocal responses without static magnetic fields.

The nonreciprocity of gyrotropic media is rooted in the magnetic field bias that forces the electrons to undergo cyclotron orbits in the bulk region. The circular motion of the charged particles creates a drag-type effect when the electrons interact with a time-varying field, which is at the origin of the

Faraday rotation in bulk gyrotropic media. A simple way to picture the wave propagation in a magnetically biased material is to imagine that the wave goes through a centrifuge, e.g., rotating drum, and is dragged by the rotation of the walls. The static magnetic field endows the material with an angular momentum.

A different paradigm for a magnetic-free nonreciprocal response was recently studied by different authors [6], [23–29], and relies on a graphene sheet with drifting electrons. In this case, a static voltage generator biases the electrons with a "linear momentum," which is manifested in the form of DC current; thus, a drift-current biased graphene may behave similarly to a moving medium [6, 27–30]. In particular, the drifting electrons may drag the graphene plasmons along the direction of motion, analogous to the Fizeau effect [31]. For large drift velocities comparable with the Fermi velocity v_F, the drag effect can be so strong that the plasmon propagation becomes unidirectional and is largely insensitive to the backscattering from obstacles or imperfections [6]. Furthermore, a drift-current biased graphene sheet is an active system because the electrons can give away their kinetic energy in the form of electromagnetic radiation [27, 29].

The electrons in graphene are described by a massless Dirac equation and behave like relativistic Dirac Fermions with a linear dispersion [32]. The peculiar electronic properties of graphene lead to rather unique features of the optical response, e.g., to a strongly spatially dispersive conductivity with a square-root singularity in the momentum space [32]. A

✉ Filipa R. Prudêncio
filipa.prudencio@lx.it.pt

1 Instituto Superior Técnico and Instituto de Telecomunicações, University of Lisbon, Avenida Rovisco Pais 1, 1049-001 Lisbon, Portugal

2 Instituto Universitário de Lisboa (ISCTE-IUL), Lisbon, Portugal

particularly attractive feature of graphene is the ultra-subwavelength nature of plasmon excitations with relatively large propagation lengths. Graphene plasmonics is expected to play an important role in the development of THz photonics [33], and may have important applications in waveguiding, biological sensing, spectroscopy, and others.

Electronic energy-loss spectroscopy (EELS) is a powerful method to characterize electronic band structures, plasmons, and the response of structured materials [34–37]. It relies on the analysis of either the electron energy losses or the emitted radiation when a beam of swift electrons travels close by (or through) some target. In particular, low-energy electron microscopy uses electrons with 1–100 eV, and enables a sub-eV energy resolution (on the order of 20 meV or less using monochromated electron beams [40]) which is fine enough to characterize low-energy excitations, such as acoustic plasmons and excitons in the infrared range [36–40]. The amount of energy loss measured via EELS depends on phonon excitations, plasmon excitations, and Cherenkov radiation [41]. Recently, the Cherenkov effect was investigated in plasmonic platforms and in metamaterials with a plasmonic-type hyperbolic response [42–49]. In particular, in ref. [49], we found out that in topological nonreciprocal plasmonic systems, the spectrum of the emitted Cherenkov radiation can be strongly dependent on the direction of motion of the electron beam.

Motivated by these developments, here we investigate how the drift-current bias of graphene may influence the power extracted from a beam of swift electrons that travel parallel to the graphene sheet. We find that the energy loss is typically boosted when the electron beam moves in the direction *opposite* to the drifting electrons. In contrast, the energy loss is negligible when the electron beam and the drifting electrons move along the same direction with similar velocities. Thus, the drift current creates a strongly asymmetric noncontact friction effect. Furthermore, we compare the energy loss predicted by different conductivity models of the drift-current biased graphene. Our calculations suggest that EELS measurements can be useful to test the validity of the available theoretical models and to characterize the dispersion of short-wavelength plasmons.

Radiation Mechanisms

In our theoretical analysis, the electron beam is modeled as a pencil beam (Fig. 1) described by the current density $\mathbf{j}(x, z, t) = -e n_y v_0 \delta(z - z_0) \delta(x - v_0 t) \hat{\mathbf{x}}$. Here, v_0 is the velocity of moving charges, $-e$ is the electron charge, n_y is the number of charges per unit of length along the y direction, and $z_0 \equiv d$ is the height of the beam relative to the graphene sheet. For simplicity, the beamwidth, measured along the z direction, is taken infinitesimally small. The problem is effectively two-
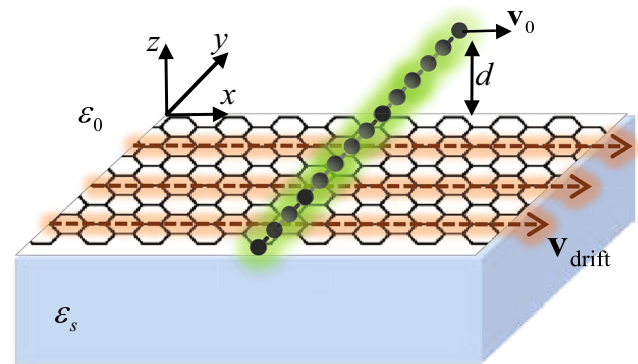

Fig. 1 A pencil beam of electrons with velocity v_0 moves nearby a graphene sheet biased with drifting electrons with a velocity v_{drift}. The graphene sheet stands on the top of a dielectric (SiO$_2$) substrate

dimensional because $\mathbf{j}$ is independent of y. It is assumed that the graphene sheet lies on the top of material substrate (e.g., SiO$_2$) with a dielectric constant $\varepsilon_s = 4$ and is biased with drifting electrons with a velocity v_{drift}. The drift current is induced by a DC voltage generator (not shown in Fig. 1).

Following ref. [49], the instantaneous magnetic field excited by the electron beam is of the form $\mathbf{H}(x, z, t) = H_y \hat{\mathbf{y}}$ with

$$H_y(x, z, t) = \frac{1}{2} n_y e \, \text{sgn}(v_0) \omega_F h_y(x, z, t)$$
$$h_y(x, z, t) = \frac{1}{2\pi} \int_{-\infty}^{+\infty} h_y(x, z, \omega) e^{-i\omega t} \frac{d\omega}{\omega_F} \quad (1)$$

where ω_F is a normalization constant with units of frequency so that $h_y(x, z, t)$ is dimensionless. The normalization constant is taken identical to $\omega_F = \mu_c/\hbar$, where μ_c is the chemical potential of the graphene sheet and $\hbar$ is the reduced Planck constant. The fields have a traveling wave-type variation in spacetime, such that $H_y(x, z, t) = H_y(x - v_0 t, z, t = 0)$. The function $h_y(x, z, \omega)$ determines the spectrum of the emitted magnetic field. In the vacuum region ($z > 0$), it can be written as

$$h_y(x, z, \omega) = \left[\text{sgn}(-z + z_0) e^{-\gamma_0 |z - z_0|} + R e^{-\gamma_0 (z + z_0)} \right] e^{ik_x x}, \quad (2)$$
$$k_x = \omega/v_0.$$

Here, $\gamma_0 = \sqrt{k_x^2 - \omega^2/c^2}$ is the z-propagation constant in free-space and $R = R(\omega, k_x)$ is the (magnetic field) reflection coefficient of the graphene sheet for plane wave incidence. In the previous formulas, the wave number k_x must satisfy the selection rule $k_x = \omega/v_0$, and thereby is indirectly determined by the energy of the swift electrons. The electric field in the air region is such that $\partial_t \mathbf{E} = \varepsilon_0^{-1} (\nabla \times \mathbf{H} - \mathbf{j})$.

By enforcing the continuity of the tangential component of the electric field $E_x|_{z=0^+} - E_z|_{z=0^-} = 0$ and the impedance boundary condition $H_y|_{z=0^+} - H_y|_{z=0^-} = -\sigma_{g,\text{drift}} E_x$, it can be

shown that [27]

$$R(\omega, k_x) = \frac{i\omega\varepsilon_0(\varepsilon_s\gamma_0 - \gamma_s) - \sigma_{g,\text{drift}}\gamma_s\gamma_0}{i\omega\varepsilon_0(\varepsilon_s\gamma_0 + \gamma_s) - \sigma_{g,\text{drift}}\gamma_s\gamma_0}, \tag{3}$$

where $\gamma_s = \sqrt{k_x^2 - \varepsilon_s\omega^2/c^2}$ is the z-propagation constant in the substrate and $\sigma_{g,\text{drift}}$ is the graphene conductivity with the drifting electrons.

One can find in the literature different theoretical models for the conductivity of graphene with a drift-current bias [23–29]. In refs. [27, 29], it was shown using distinct approaches that when the electron scattering is mainly determined by electron-electron interactions, the effect of the electric bias is ruled by a Galilean Doppler shift ($\omega \to \widetilde{\omega} = \omega - k_x v_{\text{drift}}$ and $k_x \to \widetilde{k}_x = k_x$), such that the conductivity is given by:

$$\sigma_{g,\text{drift}}(\omega, k_x) = \frac{\omega}{\widetilde{\omega}}\sigma_g(\widetilde{\omega}, k_x), \ \widetilde{\omega} = \omega - k_x v_{\text{drift}} \tag{4}$$

In the above, $\sigma_g(\omega)$ is the bare graphene conductivity (with no drift), v_{drift} is the drift velocity, $\widetilde{\omega}$ is the Doppler-shifted frequency, ω is the oscillation frequency, and k_x is the propagation constant along the x direction. The time variation $e^{-i\omega t}$ is implicit. Alternative models for the graphene conductivity were developed by other authors [23–26] relying on a shifted Fermi distribution. With a single band approximation (with the interband transitions discarded), the conductivity obtained with the shifted Fermi distribution is ruled by a relativistic-type Doppler shift in the zero temperature limit [23, 29]:

$$\sigma_{g,\text{drift}}^{R}(\omega, k_x) = \frac{\omega}{\widetilde{\omega}}\sigma_g(\widetilde{\omega}, \widetilde{k}_x), \ \widetilde{\omega} = \gamma_g(\omega - k_x v_{\text{drift}}), \widetilde{k}_x$$
$$= \gamma_g(k_x - \omega v_{\text{drift}}/v_F^2) \tag{5}$$

where $\gamma_g = 1/\sqrt{1 - v_{\text{drift}}^2/v_F^2}$ is the graphene Lorentz factor and v_F is the Fermi velocity.

As discussed in ref. [29], the shifted Fermi distribution determines a distribution of the electronic kinetic momentum, whereas the relevant distribution for the computation of the graphene conductivity with the Lindhard formula is a distribution of canonical (Bloch wave vector) momentum, which is unaffected by the drift current. Thus, in our understanding, Eq. (4) should model better the effect of the drift-current bias than Eq. (5). Intuitively, when the electron-electron collisions predominate, the electron gas is forced to move as a whole (with the drift velocity) similar to a moving medium, and thereby its conductivity is expected to be described by a standard Galilean Doppler shift transformation [27, 29]. We demonstrate later in the article that the energy-loss spectrum predicted by Eqs. (4) and (5) may differ substantially, and thereby that EELS measurements may be useful to experimentally test the validity of the theoretical models.

The bare (no drift) graphene conductivity $\sigma_g(\omega, k_x)$ is calculated analytically using [50, 51]

$$\sigma_g(\omega, k_x) = -i\omega\chi_\Gamma(\omega, q), \tag{6a}$$

$$\chi_\Gamma(\omega, q) = \left(1 + \frac{i\Gamma}{\omega}\right)\frac{\chi(\omega + i\Gamma, q)}{1 + \frac{i\Gamma}{\omega}\frac{\chi(\omega + i\Gamma, q)}{\chi(0, q)}}, \tag{6b}$$

$$\chi(\omega, q) = \frac{e^2}{4\pi\hbar}\left[\frac{8k_F}{q^2 v_F} + \frac{G(\Delta_-) - G(\Delta_+) + i\pi}{\text{sq}(\omega - v_F q)\text{sq}(\omega + v_F q)}\right], \tag{6c}$$

where Γ is the scattering rate, $k_F = \mu_c/(\hbar v_F)$ is the Fermi wave number, μ_c is the chemical potential, $\Delta_\pm = (\hbar\omega \pm 2\mu_c)/(\hbar v_F q)$ and $q = \sqrt{k_x^2}$. We rewrote the formula of refs. [50, 51] in such a way that it is an analytical function of $k_x = k_x' + ik_x''$ when k_x is near the real axis and ω is real-valued. The functions $G(z)$ and $\text{sq}(z)$ in Eq. (6c) are defined in the Appendix. The formalism assumes that $k_B T << \mu_c$. Throughout the article, we use $\mu_c = 0.1$ eV and a scattering rate equal to $\Gamma = 1/(0.35$ ps).

To begin with, we calculate the dispersion of the graphene plasmons for different drift velocities. The dispersion equation is determined by the poles of the reflection coefficient: $i\omega\varepsilon_0(\varepsilon_s\gamma_0 + \gamma_s) - \sigma_{g,\text{drift}}\gamma_s\gamma_0 = 0$ [see Eq. (3)]. For simplicity, we use a quasi-static approximation ($\gamma_0 \approx \gamma_s \approx q$), which yields $\frac{i\omega\varepsilon_0}{\sigma_{g,\text{drift}}}(\varepsilon_s + 1) - q = 0$. The dispersion diagram is found by solving this equation with respect to $k_x = k_x' + ik_x''$ as a function of a real-valued ω. The dispersion for the Galilean Doppler-shift model of the conductivity is shown in Fig. 2a for drift velocities v_{drift} on the order of $v_F = c/300$ [52, 53]. As seen, the drift bias creates an asymmetry between the +x and −x directions such that the dispersion diagram bends upwards (downwards) for waves that co-propagate (counter-propagate) with the drifting electrons, creating conditions for regimes of unidirectional propagation. Figure 2c shows the ratio of the imaginary parts (k_+'' and k_-'') of the complex propagation constant for counter-propagating plasmons and $v_{\text{drift}} = v_F/4$. Note that k_+'' and k_-'' are the attenuation constants associated with waves propagating along the +x and −x directions, respectively. As seen, the waves propagating in the direction opposite to the drifting electrons (associated with k_-'') are much more attenuated than the waves propagating along the drift direction. Thus, a drift-biased graphene sheet can effectively behave as a one-atom thick optical isolator [6, 28]. For comparison, we show in Fig. 2b the dispersion diagram obtained with the relativistic Doppler-shift model. The results are qualitatively similar to those depicted in Fig. 2a, but the effect of the drift on the dispersion of the graphene plasmons is dramatically weaker in a relativistic model. In the rest of article, except if explicitly mentioned otherwise, all the calculations are done with the Galilean Doppler-shift model of graphene Eq. (4).
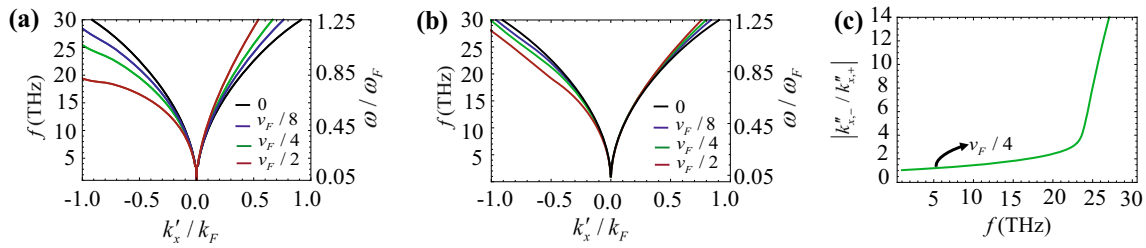
Fig. 2 **a** Dispersion diagram of the graphene plasmons (see the geometry of the structure in Fig. 1) calculated with the Galilean Doppler-shift model of graphene Eq. (4) for different drift velocities indicated in the insets. **b** is similar to **a** but calculated with relativistic Doppler-shift model [Eq. (5)].

c Ratio of the attenuation constants for counter-propagating plasmons, for $v_{drift} = v_F/4$, obtained with the Galilean Doppler-shift model. The complex propagation constant is $k_x = k_x' + ik_x''$

Let us now suppose that an electron beam interacts with the drift-current biased graphene. The moving electrons interact resonantly with the graphene plasmons that satisfy the selection rule $k_x = \omega/v_0$ [36, 50] (it is underlined that R in Eq. (2) is evaluated with $k_x = \omega/v_0$). Thus, the plasmons that can be excited by moving charges with $\pm v_0$ velocity can be found by intersecting the lines $k_x = \omega/v_0$ and $k_x = \omega/(-v_0)$ with the plasmon dispersion diagram, respectively. This is illustrated in Fig. 3a for the case of $v_{drift} = v_F/4$ and an electron beam with velocity $\pm v_0 = \pm 2v_F$; this velocity corresponds to an electron energy on the order of 11 eV. As seen, the propagation constant and oscillation frequency of the excited plasmons are strongly dependent on the sign of the velocity of moving charges v_0 due to the asymmetry of the dispersion diagram. Consistent with this property, the absolute value of the reflection coefficient $R(\omega, k_x)|_{k_x=\omega/v_0}$ is peaked at a frequency that depends on the sign of v_0 (Fig. 3b). For example, for $v_0 = \pm$

$2v_F$, $|R|$ is peaked near 13.5 THz and 37.1 THz, respectively, which are the frequencies determined by the intersection of $k_x = \pm\omega/v_0$ with the plasmon dispersion diagram.

Figures 3c and 3d depict a density plot of the spectrum of the radiated magnetic field ($h_y(x, z, \omega)$) evaluated at $\omega/2\pi = 13.5$ THz for $v_0 = \mp 2v_F$, respectively. Consistent with Fig. 3a, for $v_0 = -2v_F$, the emitted field is strongly attached to the graphene sheet ($z = 0$), which is a clear fingerprint of plasmon excitation at 13.5 THz. On the other hand, for $v_0 = +2v_F$, the emitted field at 13.5 THz is mostly concentrated near the electron beam ($z = d$).

We also calculated the instantaneous field with an inverse Fourier transform [Eq. (1)] for negative and positive values of v_0 (see Fig. 4a and b, respectively). The results reveal that when the electron beam moves in the direction opposite to the drifting electrons (Fig. 4a), the interaction with the plasmons is stronger due to the longer wavelengths of the excited

Fig. 3 **a** Dispersion diagram of the graphene plasmons for a drift velocity $v_{drift} = 0.5v_F$ (dark blue curves) superimposed on the lines $\omega = -v_0 k_x'$ and $\omega = v_0 k_x'$, with $v_0 = 2v_F$ (dashed black curves). **b** Reflection coefficient $|R|$ as a function of the frequency for the drift velocity $v_{drift} = 0.5v_F$ and an electron beam with $v_0 = -2v_F$ (solid curve) or with $v_0 = 2v_F$ (dashed curve). **c** and **d** Density plot of the real part of the normalized magnetic field spectrum $h_y(x, z, \omega)$ calculated at $\omega/2\pi = 13.5$ THz for the drift velocity $v_{drift} = 0.5v_F$ and $d = 25$ nm. **c** The electron beam propagates along $-x$ direction ($v_0 = -2v_F$). **d** The electron beam propagates along $+x$ direction ($v_0 = +2v_F$)
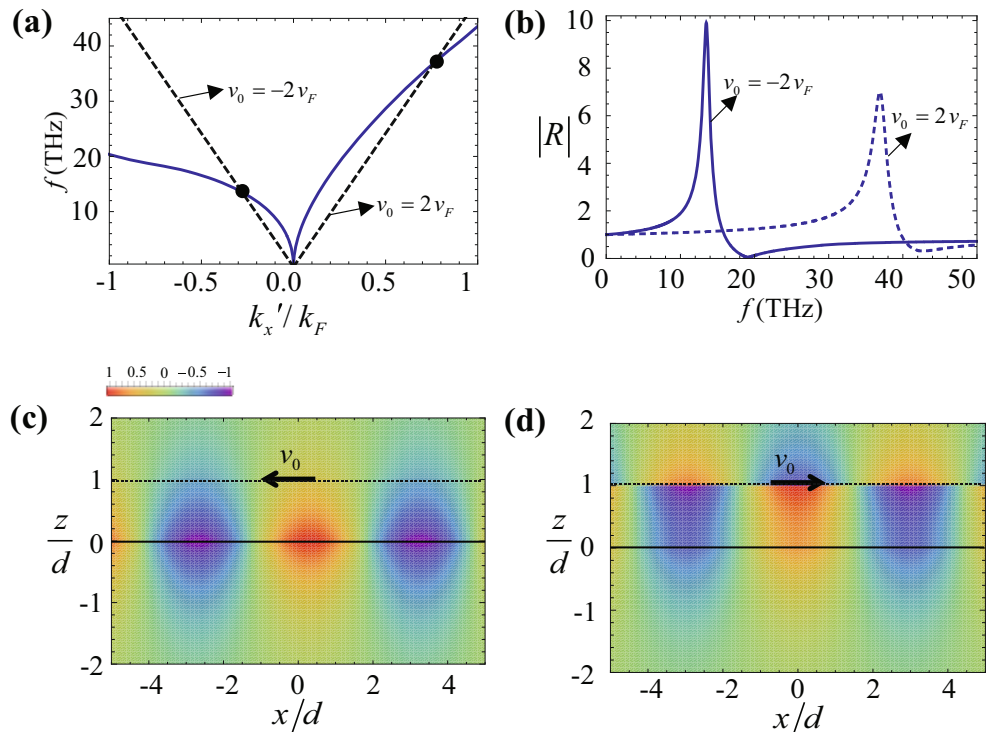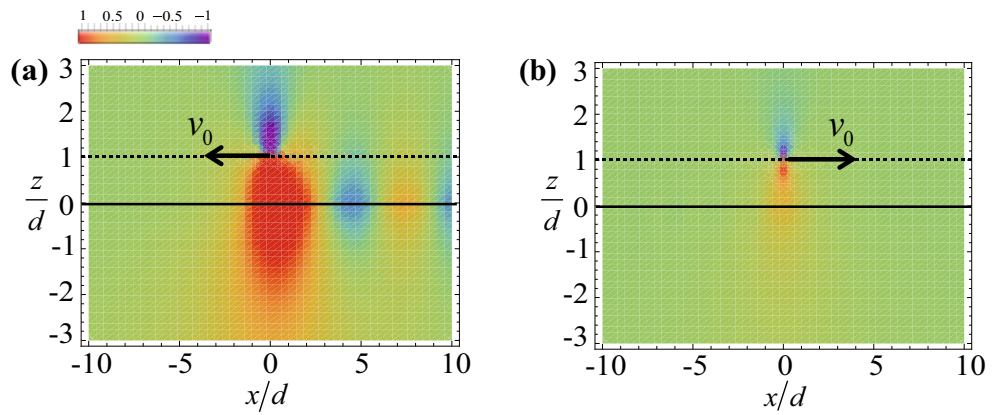
Fig. 4 Snapshot ($t = 0$) of the magnetic field intensity $H_y(x, z, t)$ (in arbitrary units) for a drift velocity $v_{\text{drift}} = 0.5 v_F$. The distance between the electron beam and the graphene sheet is $d = 25$ nm. The electron beam velocity. **a** $v_0 = -2v_F$. **b** $v_0 = 2v_F$

surface mode (see Fig. 3a). When the beam and moving electrons move along the same direction (Fig. 4b), the launched plasmons have a very short wavelength and die out quickly. This means that the resonance of $|R|$ associated with a positive v_0 (see Fig. 3b) is much more difficult to excite than the resonance of $|R|$ associated with a negative v_0. Thereby, the plasmons can be efficiently launched in the graphene only when the electron beam travels in the direction opposite to the drifting electrons. Due to this reason, the emitted radiation field depends strongly on the sign of v_0.

Electron Energy Loss

The amount of energy extracted from the electron beam can be characterized through the stopping power [29, 44, 49] $P_{\text{ext}} = -\int \mathbf{E}_{\text{loc}} \cdot \mathbf{j} \, dV$, where $\mathbf{E}_{\text{loc}}$ represents the local electric field that acts on the electron beam and $\mathbf{j}(x, z, t)$ is the electric current density. Straightforward calculations show that

$$\frac{P_{\text{ext}}}{L_y} = \frac{P_0}{z_N} \int_{-\infty}^{+\infty} G(\omega) \frac{d\omega}{\omega_F}, \tag{7}$$

where $P_0 = \frac{n_y^2 e^2}{4\pi\varepsilon_0} c$ is a normalization factor (with units of power), L_y represents the width of the current pencil along the y direction, z_N is a reference distance (which we take $z_N = 10$ nm) and

$$G(\omega) = \text{Re}\left\{-i\frac{|v_0|}{c}\gamma_0 z_N \frac{\omega_F}{\omega} R e^{-2\gamma_0 z_0}\right\} \tag{8}$$

is the (bilateral) dimensionless power spectral density of emitted radiation. The total energy loss after the electron beam travels a distance L_x over the graphene sheet is $\Delta E = P_{\text{ext}} L_x / |v_0|$. It can be written as [36]:

$$\Delta E = \int_0^{+\infty} \hbar\omega \, \Gamma_{\text{EELS}}(\omega) d\omega, \tag{9}$$

where Γ_{EELS} is the spectrum of the electron beam loss energy ($\mathcal{E} = \hbar\omega$). It has the explicit formula $\Gamma_{\text{EELS}} = \frac{A_0}{\omega_F}\Gamma_L$ where $A_0 = \frac{n_y^2 e^2}{2\pi\varepsilon_0} \frac{1}{\hbar\omega_F} \frac{L_x L_y}{z_N}$ is a dimensionless parameter and $\Gamma_L(\omega) = \text{Re}\left\{-i\gamma_0 z_N \left(\frac{\omega_F}{\omega}\right)^2 R e^{-2\gamma_0 z_0}\right\}$ is a normalized (dimensionless) spectral distribution of the energy loss.

Figure 5a depicts the power spectral density G for the electron beam velocities $v_0 = \pm 2v_F$. Clearly, the spectrum is strongly asymmetric and is peaked near the frequencies that satisfy the selection rule $k_x = \omega/v_0$, analogous to Fig. 3.

The normalized spectrum of the energy loss is represented in Fig. 5b as a function of the electron energy ($\mathcal{E} = \hbar\omega$). The black curves are computed using the conductivity obtained with the Galilean transformation Eq. (4), whereas the blue curves are calculated using the conductivity obtained with the relativistic Lorentz transformation Eq. (5). The electron energy loss is negligible when the drifting electrons and the electron beam move along the same direction (dotted curves in Fig. 5b). In contrast, when the velocities v_0 and v_{drift} have different signs (solid curves in Fig. 5b), the energy-loss spectrum exhibits a resonant peak. As seen in Fig. 5b, the peaks of Γ_L predicted by the two conductivity theoretical models do not match and can be shifted by as much as 22 meV. The reason is the relatively weak sensitivity of the graphene plasmons calculated with the relativistic conductivity model to the effect of the drift-current bias (see Fig. 2). In principle, low-energy electron microscopy may be able to distinguish such shifts, and thus EELS measurements may be instrumental to test the validity of the available theoretical models for the conductivity of graphene with a drift-current bias.

Figure 5c shows the stopping power for an electron beam with a velocity v_0 on the order of v_{drift}. Similar to Γ_L, the stopping power is negligible when v_0 has the same sign as v_{drift}. This result can be explained noting that when the electron beam moves at the same speed as the drifting electrons, their interaction is static-like and hence does not lead to any emission of radiation. In contrast, when the velocities have opposite signs, the electron beam can exchange energy with

Fig. 5 **a** Power spectral density G as a function of the frequency, for $v_{drift} = 0.5v_F$, $d = 25$ nm and (i) $v_0 = -2v_F$ (solid curve) and (ii) $v_0 = 2v_F$ (dashed curve). **b** Normalized electron-energy-loss spectrum calculated with the Galilean (black curves) and relativistic (blue curves) models of the dynamic conductivity for $\pm v_{0-} = 2v_F$. The structural parameters are the same as in panel **a**. **c** Stopping power P_{ext} (in arbitrary units) for an electron beam with v_0 on the order of v_{drift} and $d = 25$ nm. **d** Expanded representation of the stopping power P_{ext} as a function of the electron beam velocity v_0 for the values of d indicated in the insets
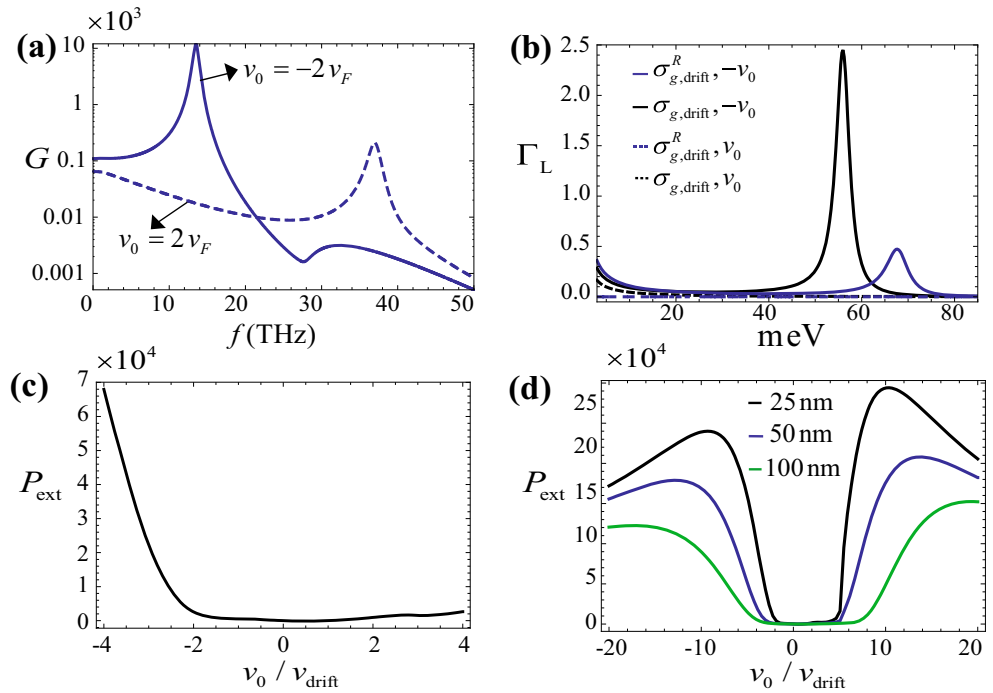
the drifting electrons in an irreversible manner due to the relative motion, leading to a strong emission of (Cherenkov-type) radiation. This loss mechanism is reminiscent of (quantum) noncontact electromagnetic friction [30, 54–57]. Note that for the example of Fig. 5c, $|v_0| = 4v_{drift}$; for this case, the stopping power for a negative beam velocity is much larger (about 34 times) than the stopping power for a positive beam velocity. Hence, the drift-current biased graphene can behave similar to a "diode" from the point of view of the electron energy loss. For values of v_0 much larger than v_{drift}, other radiation channels (different from the graphene plasmons) can predominate, and in general, the stopping power is larger when the electron beam and the drifting electrons move along the same direction (see Fig. 5d).

Finally, we study the impact of the nonlocal effects of the bare graphene conductivity on the energy-loss spectrum. Figure 6a compares the spectrum of the energy loss Γ_L calculated using Eq. (4) with the bare graphene conductivity $\sigma_g(\omega, k_x)$ given by Eq. (6) (nonlocal model) with the result obtained by neglecting the spatial dispersion in the bare graphene

conductivity $\sigma_g \to \sigma_g(\omega, q = 0^+)$ (local model). As before, the energy loss is insignificant when v_0 and v_{drift} have the same sign. In contrast, when v_0 and v_{drift} have opposite signs, the peak value of Γ_L is notoriously sensitive to the nonlocal response of the bare graphene response.

It is difficult to determine how a finite temperature affects Γ_L using the nonlocal model of $\sigma_g(\omega, q)$ as its numerical evaluation is rather intricate. To circumvent this problem and have some qualitative understanding on how Γ_L may change with the temperature, we calculated the energy loss using the local model with $\sigma_g(\omega)$ evaluated with the standard local (Kubo) formula [32]. As seen in Fig. 6b, a finite temperature weakens somewhat the light-matter interactions, but affects little the position of the peak of Γ_L.

Summary

In summary, it was shown that a graphene sheet biased with a drift electric current enables strongly asymmetric light matter

Fig. 6 Normalized electron-energy-loss spectrum Γ_L for $v_{drift} = 0.5v_F$, $d = 25$ nm, and $v_0 = \pm 2v_F$, calculated with **a** the local and nonlocal models of σ_g. **b** The local model for $T = 0$ K and $T = 300$ K
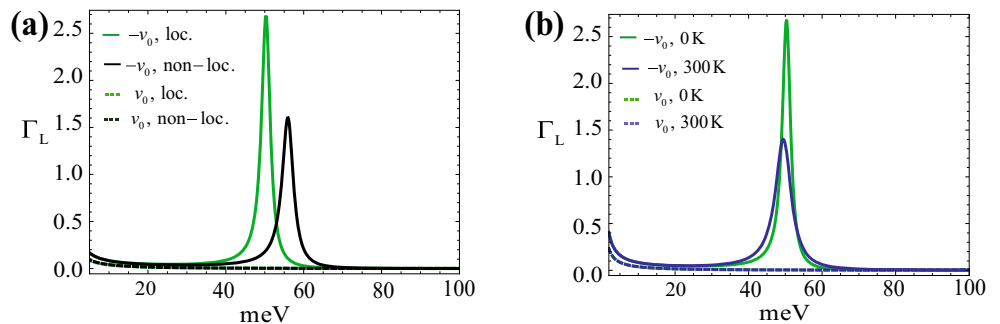
interactions that lead to an electron-energy-loss spectrum strongly dependent on the sign of the electron beam velocity. In particular, the proposed platform may behave as some sort of "Cherenkov-diode," such that the energy loss is strongly suppressed when the drift and electron beam velocities have the same sign and comparable values. When the drift and electron beam velocities have opposite signs, the light-matter interactions are boosted and result in a massive energy loss and in a noncontact friction-type effect. The role of unidirectional graphene plasmons in these effects was highlighted. It was suggested that EELS measurements may be helpful to clarify the validity of the available theoretical conductivity models of graphene with a drift-current bias, as the peaks of energy loss predicted by the different models can be shifted by as much as 20 meV.

Appendix

The function $G(z)$ in Eq. (6c) is given by:

$$G(z) = z\,\mathrm{sq}(z-1)\mathrm{sq}(z+1) \tag{10}$$

$$-\left[\ln\left((z + \mathrm{sq}(z-1)\mathrm{sq}(z+1))e^{i\theta_0}\right) - i\theta_0\right]$$

where ln represents the standard logarithm function with a branch cut in the negative real axis and $\theta_0 = -\pi/4$. The function $\mathrm{sq}(\omega)$ with $\omega = \omega' + i\omega''$ is determined by

$$\mathrm{sq}(\omega) = \begin{cases} -\sqrt{\omega}, & \text{if } \omega' < 0 \text{ and } \omega'' < 0 \\ \sqrt{\omega}, & \text{otherwise} \end{cases} \tag{11}$$

where $\sqrt{}$ is the standard square root function with a branch cut in the negative real axis.

References

1. Wang Z, Fan S (2005) Optical circulators in two-dimensional magneto-optical photonic crystals. Opt Lett 30:1989
2. Wang Z, Chong YD, Joannopoulos JD, Soljačić M (2008) One-way electromagnetic waveguide formed at the interface between plasmonic metal under a static magnetic field and a photonic crystal. Phys Rev Lett 100:012905
3. Haldane FDM, Raghu S (2008) Possible realization of directional optical waveguides in photonic crystals with broken time-reversal symmetry. Phys Rev Lett 100:012904
4. Raghu S, Haldane FDM (2008) Analogs of quantum-Hall-effect edge states in photonic crystals. Phys Rev A 78:033834
5. Lu L, Joannopoulos JD, Soljačić M (2014) Topological photonics. Nat Photonics 8:821–829
6. Morgado TA, Silveirinha MG (2018) Drift-induced unidirectional graphene plasmons. ACS Photonics 5:4253–4258
7. Prudêncio FR, Matos SA, Paiva CR (2015) Asymmetric band diagrams in photonic crystals with a spontaneous nonreciprocal response. Phys Rev A 91:063821
8. Prudêncio FR, Silveirinha MG (2016) Optical-isolation of circularly polarized light with a spontaneous magnetoelectric effect. Phys Rev A 93:043846
9. Silveirinha MG (2017) PTD symmetry protected scattering anomaly in optics. Phys Rev B 95:035153
10. Caloz C, Alù A, Tretyakov S, Sounas D, Achouri K, Deck-Léger ZL (2018) Electromagnetic nonreciprocity. Phys Rev Applied 10:047001
11. Silveirinha MG (2019) Time-reversal symmetry in antenna theory. Symmetry 11:486
12. Gallo K, Assanto G, Parameswaran KR, Fejer MM (2001) All optical diode in a periodically poled lithium niobate waveguide. Appl Phys Lett 79:314–316
13. Soljačić M, Luo C, Joannopoulos JD, Fan S (2003) Nonlinear photonic crystal microdevices for optical integration. Opt Lett 28:637–639
14. Fleury R, Sounas DL, Sieck CF, Haberman MR, Alù A (2014) Sound isolation and giant linear nonreciprocity in a compact acoustic circulator. Science 343:516–519
15. Hafezi M, Rabl P (2012) Optomechanically induced non-reciprocity in microring resonators. Opt Express 20:7672
16. Lannebere S, Silveirinha MG (2016) Wave instabilities and unidirectional light flow in a cavity with rotating walls. Phys Rev A 94:033810
17. Kodera T, Sounas DL, Caloz C (2011) Artificial Faraday rotation using a ring metamaterial structure without static magnetic field. Appl Phys Lett 99:031114
18. Wang Z, Wang Z, Wang J, Zhang B, Huangfu J, Joannopoulos JD, Soljačić M, Ran L (2012) Gyrotropic response in absence of a bias field. Proc Natl Acad Sci U S A 109:13194–13197
19. Sounas DL, Alù A (2017) Non-reciprocal photonics based on time modulation. Nat Photonics 11:774–783
20. Estep NA, Sounas DL, Soric J, Alù A (2014) Magnetic-free non-reciprocity and isolation based on parametrically modulated coupled-resonator loops. Nat Phys 10:923–927
21. Deck-Léger Z-L, Chamanara N, Skorobogatiy M, Silveirinha MG, Caloz C (2019) Uniform-velocity spacetime crystals. Advanced Photonics 1:056002
22. P. A. Huidobro, E. Galiffi, S. Guenneau, R.V. Craster, J.B. Pendry, "Fresnel drag in space-time modulated metamaterials", *PNAS* (2019), https://doi.org/10.1073/pnas.1915027116
23. D. S. Borgnia, T. V. Phan, L. S. Levitov, "Quasi-relativistic doppler effect and non-reciprocal plasmons in graphene", arXiv: 478 1512.09044 (2015)
24. Sabbaghi M, Lee H-W, Stauber T, Kim KS (2015) Drift-induced modifications to the dynamical polarization of graphene. Phys Rev B 92:195429
25. B. Van Duppen, A. Tomadin, A. N. Grigorenko, M. Polini, "Current-induced birefrigent absorption and non-reciprocal plasmons in graphene", *2D Mater.* **3**, 015011 (2016)
26. Wenger T, Viola G, Kinaret J, Fogelström M, Tassin P (2018) Current-controlled light scattering and asymmetric plasmon propagation in graphene. Phys Rev B 97:085419
27. Morgado TA, Silveirinha MG (2017) Negative Landau damping in bilayer graphene. Phys Rev Lett 119:133901
28. Correas-Serrano D, Gomez-Diaz JS (2019) Nonreciprocal and collimated surface plasmons in drift-biased graphene metasurfaces. Phys Rev B 100:081410
29. T. A. Morgado, M. G. Silveirinha, Reply to comment on "Negative Landau Damping in Bilayer Graphene", *Phys. Rev. Lett.* **123**, 219402, (2019). (see also arxiv.org/abs/1812.09103)

30. Silveirinha MG (2014) Optical instabilities and spontaneous light emission by polarizable moving matter. Phys Rev X 4:031013

31. Fizeau H (1851) Sur les hypothèses relatives à l'éther lumineaux. Comptes Rendus 33:349–355

32. Gonçalves PAD, Peres NMR (2016) An introduction to graphene plasmonics. World Scientific, Hackensack, NJ

33. Ferguson B, Zhang X-C (2002) Materials for terahertz science and technology. *Nat Mater* **1**:26–33

34. Hillier J, Baker RF (1944) Microanalysis by means of electrons. J Appl Phys 15:663–675

35. C. J. Powell, J. B. Swan, "Origin of the characteristic electron energy losses in aluminum", *Phys. Rev.* **115**, 869 (1959)

36. de Abajo FJG (2010) Optical excitations in electron microscopy. Rev Mod Phys 82:209–275

37. Polman A, Kociak M, de Abajo FJG (2019) Electron-beam spectroscopy for nanophotonics. Nat Mater 18:1158–1171

38. Rocca M (1995) Low-energy EELS investigation of surface electronic excitations on metals. Surf Sci Rep 22:1–71

39. Diaconescu B, Pohl K, Vattuone L, Savio L, Hofmann P, Silkin VM, Pitarke JM, Chulkov EV, Echenique PM, Farías D, Rocca M (2007) Low-energy acoustic plasmons at metal surfaces. *Nature* **448**:57–59

40. Hachtel JA, Lupini AR, Idrobo JC (2018) Exploring the capabilities of monochromated electron energy loss spectroscopy in the infrared regime. Sci Rep 8:5637

41. Cherenkov PA (1934) Visible emission of clean liquids by action of γ radiation. Dokl Akad Nauk SSSR 2:451

42. Veselago VG (1968) The electrodynamics of substances with simultaneously negative values εof and μ. Sov Phys Usp 10:509

43. So J-K, Won J-H, Sattorov MA, Bak S-H, Jang K-H, Park G-S, Kim DS, Garcia-Vidal FJ (2010) Cherenkov radiation in metallic metamaterials. Appl Phys Lett 97:151107

44. Fernandes DE, Maslovski SI, Silveirinha MG (2012) Cherenkov emission in a nanowire material. Phys Rev B 85:155107

45. Morgado TA, Fernandes DE, Silveirinha MG (2015) Analytical solution for the stopping power of the Cherenkov radiation in a uniaxial nanowire material. Photonics 2:702–718

46. Vorobev VV, Tyukhtin AV (2012) Nondivergent Cherenkov radiation in a wire metamaterial. Phys Rev Lett 108:184801

47. Liu F, Xiao L, Ye Y, Wang M, Cui K, Feng X, Zhang W, Huang Y (2017) On-chip integrated Cherenkov radiation emitter eliminating the electron velocity threshold. Nat Photonics 11:289–292

48. Silveirinha MG (2017) Low energy Cherenkov glow. Nat Photonics 11:269–271

49. Prudêncio FR, Silveirinha MG (2018) Asymmetric Cherenkov emission in a topological plasmonic waveguide. Phys Rev B 98: 115136

50. Lin X, Yang Y, Rivera N, López JJ, Shen Y, Kaminer I, Chen H, Zhang B, Joannopoulos JD, Soljacič M (2017) All-angle negative refraction of highly squeezed plasmon and phonon polaritons in graphene-boron nitride heterostructures. PNAS 114:6717–6721

51. Koppens FHL, Chang DE, García de Abajo FJ (2011) Graphene plasmonics: a platform for strong light-matter interactions. *Nano Lett* **11**(8):3370

52. Shishir RS, Ferry DK (2009) Velocity saturation in intrinsic graphene. J Phys Condens Matter 21:344201

53. Dorgan VE, Bae M-H, Pop E (2010) Mobility and saturation velocity in graphene on SiO2. Appl Phys Lett 97:082112

54. J. B. Pendry, "Shearing the vacuum-quantum friction", *J. Phys.: Condens. Matter* **9,** 10301 (1997)

55. Volokitin AI, Persson BNJ (2007) Near-field radiative heat transfer and noncontact friction. Rev Mod Phys 79:1291–1329

56. Silveirinha MG (2013) Quantization of the electromagnetic field in non-dispersive polarizable moving media above the Cherenkov threshold. Phys Rev A 88:043846

57. M. G. Silveirinha, "Theory of quantum friction", *New J.* Phys. 16, 063011 (2014)